Diffraction Prediction in HDR measurements

Antoine Lucat, Ramon Hegedus, Romain Pacanowski

Diffraction Prediction in HDR measurements

A. Lucat[1,3] and R. Hegedus[2] and R.Pacanowski[1,3]

[1] Institut d'Optique Gradute School, CNRS (LP2N), Universite de Bordeaux
[2] Department of Cognitive Neuroscience, Tubingen.
[3] INRIA Bordeaux Sud-Ouest

Abstract

Modern imaging techniques have proved to be very efficient to recover a scene with high dynamic range values. However, this high dynamic range can introduce star-burst patterns around highlights arising from the diffraction of the camera aperture. The spatial extent of this effect can be very wide and alters pixels values, which, in a measurement context, are not reliable anymore. To address this problem, we introduce a novel algorithm that predicts, from a closed-form PSF, where the diffraction will affect the pixels of an HDR image, making it possible to discard them from the measurement. Our results gives better results than common deconvolution techniques and the uncertainty values (convolution kernel and noise) of the algorithm output are recovered.

Categories and Subject Descriptors (according to ACM CCS):   I.3.3 [Computer Graphics]: Picture/Image Generation—Line and curve generation

In a wide variety of applications, the camera dynamic range does not permit to capture the whole dynamic range of the scene. High dynamic range (HDR) imaging [Rei10] is therefore necessary in order to fully recover the whole scene dynamic range. HDR photography merges photographies of a scene, taken at different levels of exposure, in order to increase the native camera dynamic range. HDR images are very useful because they speed up the acquisition process when using an imaging device.

A common artifact arising from the high dynamic range is that star burst patterns can be seen around highlights. This effect is due to light diffraction through the lens diaphragm, and cannot be avoided. From a metrology perspective, these diffraction patterns pollute a lot of pixels around the highlights, which cannot be taken as reliable measurements. Since the camera diffraction pattern has a very high dynamic range, the higher the image dynamic range is, the more prominent is the pollution by diffraction. More generally, even if the effect becomes less visible, high value pixels can always affect the lower value pixels through diffraction because the spatial range of diffraction is not bounded. One then has to be very careful when considering a low value pixel as a reliable measurement. This diffraction effect can be described by a convolution, to which is added a classical measurement noise.

Recovering a noisy measurement blurred by a convolution kernel (impulse response) is an issue of main interest since it focuses on removing the impact of the measuring instrument on the acquired data. The main difficulty is that it is an ill-posed mathematical problem ([TA77], p.7): a solution is not unique, may not exist, and may not be stable. In fact, if the deconvolved solution is not stable, a slight error in the data may lead to a very large error in the solution. It means that for measurement purposes, where noise is always present, recovering the true unbiased data is mathematically impossible. Yet, a wide variety of deconvolution techniques have been developed, divided into 4 major categories: Fourier based techniques (e.g., [Wie64]), constrained iterative algorithms (e.g., [RG05]), entropy maximization (e.g., [SB84]), and maximum likelihood estimation (Bayesian methods, cf. [Ric72]).

Unfortunately, none of these algorithms guarantee any certainty value for the deconvolution output because it depends on the problem unknowns [Eld05, Ric72]. In his original paper [Ric72], Richardson writes that the value of his process "can give intelligible results in some cases where the Fourier process cannot", highlighting the fact that the deconvolution techniques are not aimed at guaranteeing a measurement value. Therefore, the main issue with deconvolution algorithms is their inability at guaranteeing any bound-

aries for the recovered pixel value, in spite of a good shape of the reconstructed image. However, when doing metrology-grade measurements, uncertainties remain necessary.

We propose to tackle this problem differently by predicting and identifying the pixels in the image that are polluted by diffraction, and then discard these pixels from the measurement. Since our technique aims to classify pixels instead of recovering their original value, no pixel value is modified and therefore, we can keep track of the measurement uncertainty.

Overview of the Method. The first step is to precompute the optical impulse response (also called the point spread function, PSF) of the camera for a given setup. This computation is based on the diaphragm fitting with a proposed model, which is general enough to cover a wide variety of apertures, but also gives a closed-form solution of the PSF. Therefore, our algorithm (cf. Section 2) predicts the amount of diffraction present in the HDR image-based measurement. The algorithm is based on an incremental prediction of the effect of diffraction, from the highest to the lowest pixel values. Since recovering the true value for these pixels is too complicated, we simply discard them from the measurement. Section 3 presents results for HDR images taken with two different lenses and for two types of conditions (laboratory and night). Finally, we discuss some potential future work (cf. Section 4) to improve further our results.

1. Fourier Optics and Lens Diaphragm Model

As stated by Fourier Optics [Ers06], the PSF is the function that blurs a perfect incoherent image I^*, such that the captured image I is given by

$$I = I^* \otimes PSF + \mathcal{B} \tag{1}$$

with $\otimes$ the convolution operator, and $\mathcal{B}$ the measurement noise.

The PSF function is related to the camera, approximated by a thin-lens model, through

$$PSF(x,y) = \frac{1}{\lambda^2 D^2 S_{pup}} \left| \mathcal{F}[P]\left(\frac{x}{\lambda D}, \frac{y}{\lambda D}\right) \right|^2 \tag{2}$$

with $\mathcal{F}[\cdot]$ the Fourier transform operator, λ the scene wavelength, D the sensor-lens distance, (x,y) the position on the sensor, P the pupil function, and S_{pup} its area. The most important feature is that the PSF function is directly shaped by the Fourier transform of the diaphragm shape. Consequently, if we want to correctly predict diffraction effects, we need a good description of the pupil function.

The great majority of lens diaphragms are designed with blades, also known as bladed apertures. In the case of a circular diaphragm, the resulting PSF is the well-known Airy pattern. Shung-Wu and Mittra [SM83] have studied diaphragms with polygonal shapes but only for straight edges.
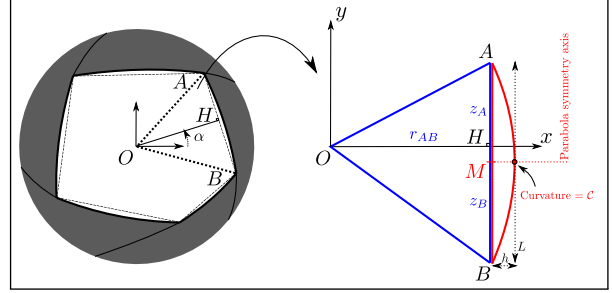

Figure 1: Mathematical model of a standard *n*-bladed camera aperture. The full pattern can be divided into similar geometries, themselves sub-divided into two elementary parts : a triangle *OAB* (blue), and a section of parabola whose axis of symmetry passes by the middle point *M* (red).

However, by construction, each blade is an arc of a circle, thus its shape is of constant curvature, giving a good description for any edge of the diaphragm. Generally, if two consecutive blades cross each other in a certain point, referred as a vertex in the following, the shape described by the set formed by these points is an irregular polygon (cf. Fig. 1). If one could think that an aperture is designed to fit a regular polygon, it is not the case because of mechanical constraints between blades, mostly when they are tight at high f-numbers. Our model also has the benefit of giving a closed-form solution of the PSF equation (cf. Eq. 2).

Algorithm 1 Diffraction detection algorithm

1: **procedure** DETECTDIFFRACTION($I_{hdr}, PSF, \rho, \mathcal{D}_b$)
2:     $I_{hdr} \leftarrow I_{hdr} / \max(I_{hdr})$
3:     $\mathcal{N} \leftarrow \text{ceil}(\log(1/\min(I_{hdr}))/\log(\mathcal{D}_b))$
4:     $\widetilde{PSF}, \mathcal{K} \leftarrow \mathcal{K}\_\text{REMOVAL}(PSF, \mathcal{D}_b)$
5:     **for** $k \leftarrow 2, \mathcal{N}$ **do**
6:         $\mathbb{1}_k \leftarrow (\mathcal{D}_b^{1-k} \geqslant I_{hdr} > \mathcal{D}_b^{-k})$
7:         $\mathbb{1}_{1 \to k-1} \leftarrow (I_{hdr} > \mathcal{D}_b^{1-k})$
8:         $I_k \leftarrow I_{hdr} * \mathbb{1}_k$
9:         $I_{1 \to k-1} \leftarrow I_{hdr} * \mathbb{1}_{1 \to k-1}$
10:       $Simu \leftarrow I_{1 \to k-1} \otimes \widetilde{PSF}$
11:       $Discarded \leftarrow Discarded$ OR $[\mathbb{1}_k$ AND $(Simu > \rho I_k)]$
12:     **end for**
13:     **return** $Discarded, \mathcal{K}$
14: **end procedure**

---

2. Diffraction Detection Algorithm

Our analytical PSF function permits to predict the effects of diffraction. From this knowledge, our algorithm simulates a second diffraction on the acquired image (the perfect image is then diffracted once by the physical diaphragm, then through simulation). Our method relies on two ideas: **(i)** if

---
Algorithm 2 Residual kernel removal

1: **procedure** $\mathcal{K}\_$REMOVAL$(PSF, \mathcal{D}_b)$
2:     $Within \leftarrow PSF \geqslant \max(PSF) / \mathcal{D}_b$
3:     $s \leftarrow \text{argmin}[\|\rho - \iint PSF * (PSF < s)\|^2]$
4:     $BottomUp \leftarrow PSF \geqslant s$
5:     $Mask \leftarrow Within$ OR $BottomUp$
6:     $\widetilde{PSF} \leftarrow PSF *!Mask$
7:     $\mathcal{K} \leftarrow PSF * Mask$
8:     **return** $\widetilde{PSF}, \mathcal{K}$
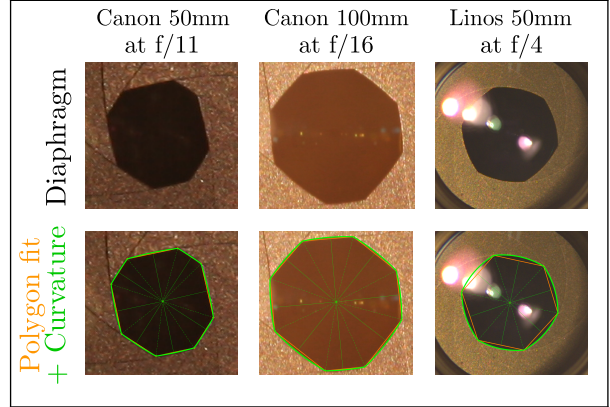9: **end procedure**

Figure 2: Fitting of our diaphragm model for different real diaphragms. The second row shows a fit with straight edges (orange) and with curved edges (green). These examples demonstrate the importance of being able to represent irregular polygonal shapes (high f-number), but also curved shapes (low f-number).

a pixel is not modified during our simulated diffraction, it was also not the case during the physical diffraction; and **(ii)** diffraction pollution on a pixel is always coming from pixels of higher values.

Our diffraction detection algorithm is divided into three parts:

1. The HDR image is cut into non-overlapping bands of values of same dynamic range $\mathcal{D}_b$.
2. A residual convolution kernel $\mathcal{K}$ is removed from the diffraction prediction (cf. Algo. 2).
3. Diffraction is progressively predicted, by iterating from the band of highest values toward the lowest and applying a user thresholding criterion to discard pixels affected by diffraction (cf. Algo. 1).

The key idea of our algorithm is that for most lenses, the dynamic range in which the PSF is very similar to a Dirac function is big, between a factor of 10 to 1000. Each band is therefore composed of two separate contributions: its inner value that is considered diffraction-free and a diffraction term coming from the higher bands. Then, convolving the measurement I by the PSF should not modify the diffraction-free pixels if they were not affected by diffraction during the measurement. Indeed, for a given band of value, the inner value is not truly free from diffraction. A certain residual kernel of diffraction cannot be detected, noted $\mathcal{K}$ (cf. Algo. 2). Therefore, our algorithm (cf. Algo. 1) essentially consists of a sequence through the bands, from the highest values to the lowest. In each iteration, a partial HDR image is convolved with the PSF, and these values are compared to the original picture, a thresholding criterion ρ is applied to distinguish clean pixels from the ones affected by diffraction. This method is then iteratively applied until the full image dynamic range has been covered. Finally, the output of the algorithm is a mask giving the pixels polluted by diffraction, and a residual convolution kernel $\mathcal{K}$. Therefore, the remaining (i.e., non-discarded) pixels I_{output} are metrologically characterized by

$$I_{output} = I^* \otimes \mathcal{K} + \mathcal{B} \quad . \tag{3}$$

3. Results

Real Aperture Fitting and Point Spread Function. The aperture model composed of an irregular polygon with curved edges is assessed to be general enough to cover a wide range of camera lenses. We tested it on our available camera lenses: one scientific-class lens of focal 50mm from Linos, and two consumer Canon lenses of 50 and 100mm focal length. The goal is to compare how the diaphragm model fits a real aperture, and to demonstrate that the resulting theoretical PSF also fits well a true PSF image.

The variety of diaphragms in Figure 2 highlights the need to have an elaborated enough mathematical modeling. Our model allows a very good fit of a wide range of common diaphragms. Furthermore, our diaphragm model gives an analytical solution of its Fourier transform, thus the resulting PSF. As shown in Figure 2, the irregular polygon and the curved edges features have their importance. For the Canon 100mm lens at f/11, it is sufficient to fit an irregular polygonal shape, with no need for a curvature term. In contrary, the Linos 50mm at f/4 could not have been described with a regular polygon, as the curvature of the edges really needs to be taken into account. Our diaphragm model fits well the aperture and we also obtain from the theory (cf. Eq. 2) a well fitted PSF compared to a real photography (cf. Figure 3).

Diffraction Prediction on HDR images. The algorithm seems to discard a lot more pixels than one would expect, highlighting the fact that the method does not pretend to discard only pixels affected by diffraction, but also diffraction-free pixels. Since the algorithm can be too conservative, the percentage of discarded measurements can significantly decrease the efficiency of an HDR image-based measurement,
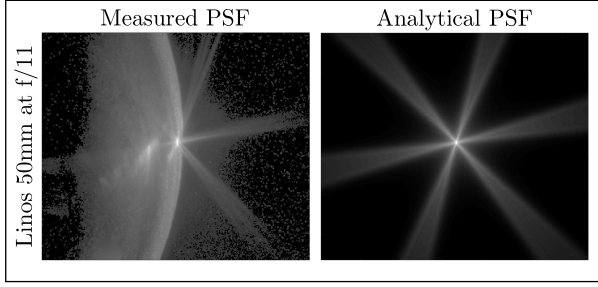
Figure 3: Comparison of the PSF resulting from the fitted diaphragm against a real HDR photograph of a quasi-point light source. Some slight differences can be observed in the repartition of light within the widened star branches of the PSF, which is explained by the random variations along the diaphragm edges that we do not take into account.
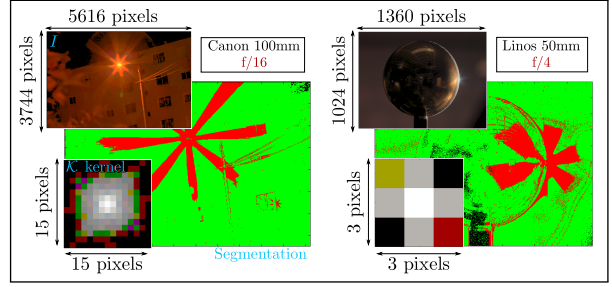

Figure 4: Results of the algorithm applied on real HDR images (tonemapped with Drago [DMAC03]) for various camera configurations, with input parameters $\mathcal{D}_b = 10$ and $\rho = 5\%$. The wavelengths used for each color channel are $[\lambda_R, \lambda_G, \lambda_B] = [600\,\mathrm{nm}, 540\,\mathrm{nm}, 470\,\mathrm{nm}]$. The segmentation images show the discarded pixels (red), the valid pixels (green), and the under-exposed ones (black). If the HDR images exhibits obvious star shaped patterns, the algorithm detects it, and they are finally removed.

ruining the benefit of having higher camera resolutions. The $\mathcal{K}$ kernel is also greatly smaller than the PSF kernel, to a range of few pixels, which guarantees that the long-range blurring effect of the PSF has been removed.

In laboratory conditions, where we used our Linos lens, the scene is perfectly stable and controlled, and the camera response is also very stationary. In this situation, shown in Figure 4, our diffraction removal algorithm completely removes the widened star shaped pattern making it very useful for measurements. In an uncontrolled scenario, (e.g., with outdoor imaging, the illumination conditions are not stable wrt. time) HDR values can be shifted up or down because of the intensity variation of lamps. Moreover, the diaphragm fitting is not guaranteed to be correct because of the repeatability of the camera lens diaphragm can be bad (especially for high f-numbers). Then, the PSF prediction is biased, so are the discarded pixels. This is visible on the left case of Figure 4, where the removed pixels seem tilted from the star shaped pattern, emerging from the lack of diaphragm repeatability.

Error Analysis A good way to quantify the quality of the separation between polluted and non-polluted pixels by diffraction is to test the algorithm on a great variety of generated HDR images. Given one image, its "real" measurement is simulated by convolving it with the precomputed PSF and by adding a Gaussian white noise, we then apply our algorithm to newly created image.

In order to remain as general as possible, our test HDR images are tuned by their bandwidth limit (Gaussian speckle pattern), their histogram of magnitude, and their HDR dynamic ($\mathcal{D}_{hdr}$). With such generated images, it is possible to generate a wide variety of images. Since the different features and conclusions do not seem to be altered whatever the input image, by default, the chosen generated image is a HDR image with a flat histogram, $\mathcal{D}_{hdr} = 10^{10}$ and a speckle size of 20 pixels.

Since our method focuses on guaranteeing no diffraction pollution on the remaining pixels, the data of interest is the histogram of relative errors between the "true" image and the "measured" one. One particular metric can be considered, the "maximum error of magnitude", noted $\mathcal{E}_{max} = \max(\mathcal{E})$, with

$$\mathcal{E} = |\log_{10}(I_{output}) - \log_{10}(I^*)| \quad . \quad (4)$$

This metric allows sorting the different methods, comparing our method to the ones from the state of the art. In Figure 5 is plotted a relative histograms of the $\mathcal{E}$ error. The PSF used to simulate the measurement is that of the 50mm Linos lens at f/11.

As firstly stated, the conclusion does not depend on the image content: the maximum error $\mathcal{E}_{max}$ resulting from our algorithm (with $\mathcal{D}_b = 10$ and $\rho = 5\%$) is always better than any other tested deconvolution method (Fig. 5, blue curves), and the result histogram (red curve) fits very well what we expect to recover (a measurement quality up to a $\mathcal{K}$ kernel convolution: equation (3), brown curve).

Figure 5 puts also in evidence that not considering diffraction may lead to a very wrong measurement: the quality of the ground truth (green curve) is far off the real initial measurement (black curve).

4. Conclusion and Future Work

We have introduced an algorithm that predicts diffraction in the case of HDR imaging measurements. The result of the algorithm ensures a good quality of the measurement, yet the link between the algorithm parameters and the resulting image characteristics is not known, despite clues on their dependence. As future work, we intend to focus on the precise
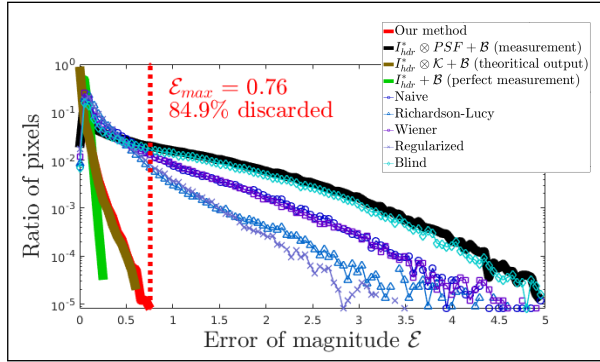
Figure 5: Histograms of the error of magnitude against a virtual reference (SNR=10) of the remaining valid pixels for different methods. The histogram of our method (red curve) is much more concentrated on the small errors than every deconvolution algorithm (blue curves). Of course, the quality of the original image (green curve) is not reached because of the residual kernel contribution, but our output error matches very well with the achieved output (brown curve) prediction.

analysis of the impact of the input image on the result. The histogram, the frequency content and the spatial coherence of the HDR image should give more insight on how to predict well the resulting error from any measurement; at the moment we still have to infer it from a generated content-equivalent image. The PSF model can also be improved, by improving the diaphragm edge description. In particular, a roughness term may be added for the edges, a method that could be inspired from the prediction of radio wave propagation above rough landscapes [Dur09].

Acknowledgements

Funding Information

References

[DMAC03] DRAGO F., MYSZKOWSKI K., ANNEN T., CHIBA N.: Adaptive Logarithmic Mapping For Displaying High Contrast Scenes. *Computer Graphics Forum 22*, 3 (sep 2003), 419–426. 4

[Dur09] DURGIN G.: The Practical Behavior of Various Edge-Diffraction Formulas. *IEEE Antennas and Propagation Magazine 51*, 3 (jun 2009), 24–35. 5

[Eld05] ELDAR Y.: Robust Deconvolution of Deterministic and Random Signals. *IEEE Transactions on Information Theory 51*, 8 (aug 2005), 2921–2929. 1

[Ers06] ERSOY O. K.: *Diffraction, Fourier Optics and Imaging*. 2006. 2

[Rei10] REINHARD E.: *High dynamic range imaging : acquisition, display, and image-based lighting*. Morgan Kaufmann/Elsevier, 2010. 1

[RG05] RIETDORF J., GADELLA T. W. J. T. W. J.: *Microscopy techniques*. Springer, 2005. 1

[Ric72] RICHARDSON W. H.: Bayesian-Based Iterative Method of Image Restoration*. *Journal of the Optical Society of America 62*, 1 (jan 1972), 55. 1

[SB84] SKILLING J., BRYAN R. K.: Maximum entropy image reconstruction: general algorithm. *Monthly Notices of the Royal Astronomical Society 211*, 1 (nov 1984), 111–124. 1

[SM83] SHUNG-WU LEE, MITTRA R.: Fourier transform of a polygonal shape function and its application in electromagnetics. *IEEE Transactions on Antennas and Propagation 31*, 1 (jan 1983), 99–103. 2

[TA77] TIKHONOV A. N. A. N., ARSENIN V. I. V. I.: *Solutions of ill-posed problems*. Winston, 1977. 1

[Wie64] WIENER N.: *Extrapolation, interpolation, and smoothing of stationary time series with engineering applications*. Technology Press of the Massachusetts Institute of Technology, 1964. 1